Why Does Insect Antifreeze Protein from *Tenebrio molitor* Produce Pyramidal Ice Crystallites?

Christina S. Strom,* Xiang Yang Liu,* and Zongchao Jia†
*Biophysics and Micro/Nanostructures Lab, Department of Physics, Faculty of Science, National University of Singapore, Singapore 117542; and †Department of Biochemistry, Queen's University, Kingston, Ontario K7L 3N6, Canada

ABSTRACT The antifreeze protein (AFP) reduces the growth rates of the ice crystal facets. In that process the ice morphology undergoes a modification. An AFP-induced surface pinning mechanism, through matching of periodic bond chains in two dimensions, enables two-dimensional regular ice-binding surfaces (IBSs) of the insect AFPs to engage a certain class of ice surfaces, called primary surfaces. They are kinetically stable surfaces with unambiguous and predetermined orientations. In this work, the orientations and molecular compositions of the primary ice surfaces that undergo growth rate reduction by the insect AFPs are obtained from first principles. Besides the basal face and primary prism, the ice surfaces engaged by insect AFPs include the specific ice pyramids produced by the insect AFP *Tenebrio molitor* (TmAFP). TmAFP-induced pyramids differ fundamentally from the ice pyramids produced by fish AFPs and antifreeze protein glycoproteins (AFPGs) as regards the ice surface configurations and the mode of interaction with the protein IBS. The molecular compositions of the TmAFP-induced pyramids are strongly bonded in two dimensions and have the constant face indices (101). In contrast, the molecular composition of the ice pyramids produced by fish AFPs and AFPGs are strongly bonded in only one direction and have variable face indices (h 0 l), none of which equal (101). The thus far puzzling behavior of the TmAFP in producing pyramidal crystallites is fully explained in agreement with experiment.

INTRODUCTION

The antifreeze proteins (AFPs) have evolved to meet the special task of protecting small water and land animals, as well as some plants, from freezing. Their special mode of interaction with the ice lattice suppresses the freezing point of water by up to several degrees. AFPs act in two stages (1–4). At the first stage, they inhibit ice nucleation, since that is a precursor to ice growth. There is evidence that fish AFPs bind to and reduce the efficiency of ice nucleators, rather than binding to embryonic ice nuclei (1). Similar phenomena as described by Wilson and Leader (1) have been obtained and explained by Du and Liu (2), Du et al. (3), and Liu and Du (4), describing how nucleation inhibition is accomplished by terminating the relevant kinetics.

The observation of some small ice crystals found in limited numbers in the bellies of fish in subzero water indicates that, despite the growth of small ice crystallites, nucleation inhibition has nevertheless occurred, albeit with a limited degree of success. Had ice nucleation been allowed to proceed unchecked, ultimately the accumulated amounts of ice crystallites would be much larger than the observed amounts.

Thus at the second stage, in cases where inhibition of ice nucleation has had partial or no success, the AFPs proceed to inhibit the growth of ice. Growth inhibition is attained by reduction of the growth rates of the crystal faces occurring in the ice morphology. Strictly speaking, a complete halt of the growth of ice would amount to the growth rates of all the ice growth fronts becoming zero. Thus in theory, if the growth inhibition were successful for 100%, very few crystallites would be observed.

A substantial curtailment of the growth of ice would amount to a substantial reduction of the absolute size of the ice crystallites. This is a commonly occurring phenomenon, as evidenced by the relatively small sizes of the ice crystals found in the bellies of fish in subzero environments. When the growth rates are reduced without actually dropping to zero, the various growth fronts experience a delay in their advance. The more severe the growth delay, the smaller the size of the resulting crystallites, and the more successful the freezing inhibition. In studying here in practice the resulting crystallites, as modified by the AFP action, we are in effect working within a framework where the AFP-induced growth inhibition is incomplete, resulting in varying degrees of growth rate reduction.

If all facets are inhibited by equal proportions, then the crystallites will be smaller but will retain the same shape; however, preferential inhibition of some surfaces over others will lead to both smaller crystallites and a modified shape. When the growth inhibition effect is marginal in less successful AFP attempts, the final crystallite size would not be very different from the original size, since the overall absolute values of the growth rates would not have decreased by much. Nevertheless the AFP action could well affect some ratios between the growth rates without reducing their absolute values by a large amount. The resulting crystallites would retain close to their normal original size, while at the same time they might exhibit a radically modified morphology.

To determine the final morphology, one needs to know the face indices and the ratios between pairs of growth rates of

Submitted November 29, 2004, and accepted for publication March 29, 2005.
Address reprint requests to Xiang Yang Liu, E-mail: phyliuxy@nus.edu.sg.

0006-3495/05/10/2618/10 $2.00
doi: 10.1529/biophysj.104.056770

the faces. But to determine the final size of the crystallite, one needs to know the absolute growth rates. Whereas the activity (i.e., strength or degree of success) of the AFP antifreeze action is reflected in the overall size of the resulting crystallite, the topological nature of the AFP action is reflected in the morphological modification—or lack of modification—induced on that crystallite. As will be detailed below, the topological nature of the AFP-ice interaction amounts to either one-dimensional periodic bond chain (PBC) matching (5), triggering secondary crystal faces (category ii below), or two-dimensional PBC matching, enhancing preferentially primary crystal faces (category i below). This work will concentrate on the latter effect while focusing on the pinning mechanism. The interaction between the protein ice binding surface (IBS) and the ice substrate determines independently both the crystallite morphology and the AFP activity. Nevertheless, no direct relation between morphology and activity need be expected on theoretical grounds, and none is conclusively observed in experiments. The conclusion is justified that the AFP-induced modification of the ice morphology is the visible manifestation rather than the cause of the freezing inhibition.

In the literature, the appearance of a disk-type ice morphology has been associated exclusively with the presence of insect AFPs that exhibit a high level of activity, whereas pyramidal forms have been associated with the presence of fish AFPs and antifreeze protein glycoproteins (AFPGs) that have a lower level of activity. The appearance of ice bipyramids in the presence of the AFP of the insect *Tenebrio molitor* (TmAFP) posed an apparent contradiction.

To resolve the specific puzzle posed by the crystallites produced by the TmAFP, one must rely on a basic formulation capable of determining from first principles the face orientations, molecular compositions, and relative growth rates of a crystal, as well as the ways these become modified by external factors like the AFP. It is necessary to compare the orientations, molecular compositions, and growth rates of the ice surfaces before and after the AFP action. Such a comparison involves, as a first prerequisite, a theoretical treatment of the mechanisms producing and modifying the crystal morphology.

Previous AFP studies have suffered from two main drawbacks: first, processes pertaining to crystal growth, as opposed to equilibrium processes, did not receive due attention (the AFP-ice-water system has been studied by molecular dynamics simulations that are normally applicable in equilibrium situations); second, crystal growth mechanisms (6) giving rise to or modifying the face orientations, the surface molecular compositions, and the relative growth rates were not properly studied.

The crucial distinction between kinetically stable surfaces and kinetically less stable or completely unstable surfaces was not appreciated (7–9). The class of kinetically stable surfaces, that is, the primary surfaces, grows through two-dimensional nucleation or spiral growth (6). The existing nonzero step-free energy in two nonparallel crystallographic directions forces the growth on such surfaces to proceed slowly, layer-by-layer, resulting in well-defined unique orientations, giving the surfaces a flat appearance. The class of kinetically less stable or totally unstable surfaces lacks a two-dimensional nucleation barrier and grows either too fast to feature in the morphology or leads to molecularly roughened surfaces.

In general, the crystallographically valid and morphologically significant surfaces are the so-called primary surfaces, i.e., surfaces bonded strongly in intersecting directions (cf. Fig. 1) (7,8). Previous AFP studies did not appreciate the fact that such surfaces are limited in number (10–12). In studying the AFP-ice system, the ice substrates considered available for the AFP action were produced by cutting randomly the hexagonal ice structure and juxtaposing the AFP ice-binding surface to those planar cut substrates, without calling to question the crystallographic validity of the randomly obtained planar cut surfaces (13). Not infrequently, surfaces were used that are either kinetically totally unstable or molecularly roughened and in either case incapable of slow layer-by-layer growth (9). Consequently the obtained results were incorrect or inconclusive at best.

PBC theory of Hartman and Perdok (7–12,14–18) enables us to reach a comprehensive explanation of the experimentally observed indices of the ice facets, as well as the mechanisms causing the AFP-induced morphological modifications. The AFP action on the bare ice substrates is considered to be the major external factor affecting the morphology. The hexagonal ice surfaces were classified according to the PBC theory in the following categories:

i. Primary surfaces, as illustrated in Fig. 1, are parallel to two or more intersecting strong-bonding directions. The face is indicated by a dashed box, and the face indices (*hkl*) are predetermined by the intersecting PBC directions A and B. A primary surface has a crystallographically valid molecular composition because it meets the so-called ''flatness'' condition (8–12): each pair of identical molecules in that growth layer differ

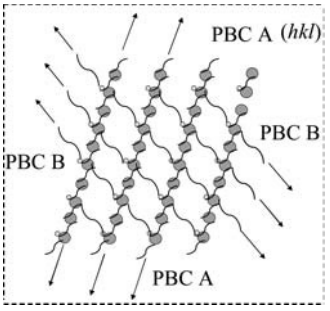

FIGURE 1 Schematic illustration of a kinetically stable primary surface (i) featuring in crystal morphology, drawn face-on. Its molecular composition consists of at least two intersecting PBCs in directions *A* and *B*, both parallel to (*hkl*), as outlined by dotted boxes. Growth units (molecules) are related by lattice translations parallel to the growing surface (conforming to the flatness condition).

by lattice translations parallel to (*hkl*). For that reason it is kinetically stable and can grow by means of a spiral growth mechanism or two-dimensional nucleation.

ii. Secondary surfaces, as illustrated in Fig. 2, are parallel to a single strong-bonding direction. Such a surface would arise if, e.g., one of the two intersecting PBCs (A and B) in the primary surface of Fig. 1 were to be removed by eliminating its constituent bonds between the molecules. E.g., when PBC A is removed from Fig. 1 but PBC B remains intact, a surface is parallel to a single strong-bonding direction, as seen in Fig. 2. Such a surface has variable, and hence adjustable, surface orientations. The reason is that a single PBC direction is parallel to infinitely many faces, e.g., $(hkl)_1$, $(hkl)_2$, etc., indicated in Fig. 2 by dashed boxes, making the face indices indeterminate. Secondary surfaces of relatively low crystallographic face indices are structurally capable of becoming kinetically stabilized under certain conditions.

iii. Surfaces not parallel to any strong-bonding directions at all are kinetically totally unstable and morphologically irrelevant. Such a surface cannot be ascribed any unique or definite face indices, as illustrated in Fig. 3.

iv. Surfaces parallel to two intersecting strong-bonding directions, but having crystallographically invalid molecular compositions, are incapable of growing according to a layer mechanism. The reason is that, again, they lack a unique, well-defined orientation. Such a flatness-violating surface configuration is schematically illustrated in Fig. 4, where some molecules (shown enlarged in the figure) differ from other identical molecules by lattice translations that are oblique to the surface. Such surfaces are molecularly roughened; cf., e.g., the discussion of (111) in the following sections.

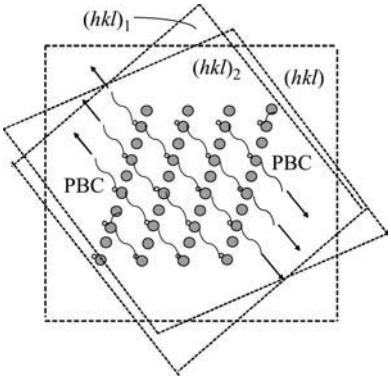

FIGURE 2 Schematic illustration of a secondary surface (ii), structurally capable of becoming kinetically stabilized as to feature in the morphology, drawn face-on. Its molecular composition consists of only one PBC. Now infinitely many faces (*hkl*), $(hkl)_1$, $(hkl)_2$, etc., outlined by dotted boxes are parallel to the PBC direction, making the surface orientation indeterminate.

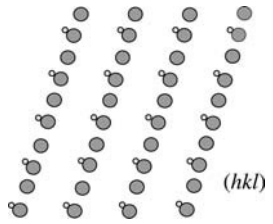

FIGURE 3 Schematic illustration of a kinetically unstable and crystallographically irrelevant surface (iii), drawn face-on. Its molecular composition contains no strong-bonding directions at all.

As can be seen in Fig. 5, the two-dimensional ''insect-type'' IBS is a rigid, planar, and repetitive structure with regularly spaced binding intervals in two directions (19,20). Experimentally this IBS correlates with the primary ice facets of category i, exemplifying surface pinning through the two-dimensional PBC-matching mechanism to be treated in this work. The IBS of fish AFPs and AFGPs, on the other hand, has binding sites that are either one dimensional with regularly and linearly arranged binding intervals or two dimensional but lack a regular arrangement of binding sites. Experimentally this IBS correlates with the secondary ice facets of category ii, exemplifying the one-dimensional PBC-matching mechanism treated in an earlier study (5). This study relies on an application of the PBC theory of crystal growth and morphology (7–12,14–18) to arrive at a comprehensive explanation of the crystallite morphology observed by insect AFPs including TmAFP.

THEORY

Overview of PBC theory

PBCs (7–12,14–18) are uninterrupted chains of strong bonds in well-defined crystallographic directions. A primary surface, category i in the Introduction,

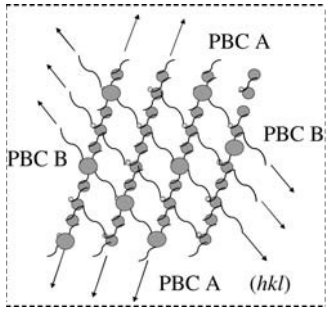

FIGURE 4 Schematic illustration of a flatness-violating or molecularly roughened surface (iv), drawn face-on. Even though the presence of two intersecting PBCs defines geometrically a face (*hkl*), the growth units (molecules) making up the molecular composition differ by lattice translations oblique to the surface (larger units are above the face differing by lattice translations from the smaller growth units that are below the face). For that reason the depicted surface configuration is crystallographically invalid.

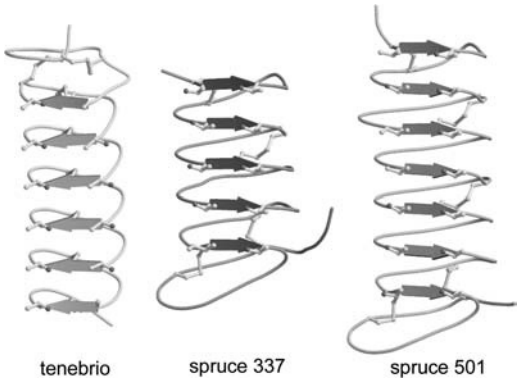

FIGURE 5 Two-dimensional IBS of the ''insect type'': TmAFP AFP (*right*) and spruce budworm AFP (*left*).

is parallel to (at least two) intersecting PBCs—$[uvw]_1$ and $[uvw]_2$—so it has a fixed surface orientation $(hkl) = [uvw]_1 \times [uvw]_2$. The layer-by-layer growth mechanism is attributed to the two-dimensional network of strong bonds in (*hkl*) formed by the intersecting PBCs. The growth layer is generated by repeated lattice translations along (*hkl*) of a basic block of equivalent molecular content as the unit cell and has thickness d_{hkl}.

An essential property is the crystallographic condition of ''flatness'' (7–12,14–18) responsible for layer growth and the emergence of flat surfaces in crystals: the basic unit cell generating the (*hkl*) growth layer should not contain lattice translations oblique to the (*hkl*) growth front (Fig. 1). As illustrated by the surfaces of category iv in Fig. 4, the violation of the flatness condition results in roughened growth, because growth units can be freely deposited in subsequent layers before the underlying layers can be completed. Because the lattice translations in such surfaces are not restricted to be parallel to the face, the deposition of growth units on the crystal face is not limited to directions parallel to that face. Growth units are deposited simultaneously not only in locations on the crystal face but also in locations away from that face. Consequently columns of growth units oblique to the face arise, and thus such surfaces cannot follow a strict layer-by-layer growth mechanism. Roughened growth is the result. Moreover, the so-called secondary surfaces in category ii (Fig. 2) possess only one strong-bonding direction. As a rule they can experience accelerated growth and will soon disappear from the growth form, even if they did occur at the beginning.

The PBC theory prescribes a progression of factors determining the observed morphology, since the observed morphology is a composite effect of internal and external factors. First, the internal factor ''structure'' is responsible for a basic theoretical morphology, known as the structural or vacuum morphology and consisting of theoretical F-faces. A basic theoretical morphology can be derived (7–12,14–18) from the primary surfaces, category i (Fig. 1). Second, the interaction between the environment and the theoretical F-faces causes a modification on the basic morphology; that modification is characterized by the properties of the environment. Usually, but not necessarily, the environment is the surrounding liquid.

Moreover, when that liquid contains influential molecular species, a further modification of the morphology may ensue. Such species may exert an even stronger morphological effect than the liquid itself, as is the case with the AFP. An example of the influence of an external factor is the kinetic stabilization by the AFP of the secondary surfaces, in category ii (5).

The attachment energy is the amount of energy released per unit cell content per mole when a new layer (*hkl*) attaches itself to the structure. It equals the sum of the interactions of the unit cell of the outermost slice with an infinite parallel stacking of slices underlying the outermost slice. The surface energy is the amount of work necessary to split a crystal isothermally and reversibly into two half crystals, producing the surfaces (*hkl*) and $(-h-k-l)$. The specific surface energy is the surface energy per unit area on the face (*hkl*).

The habit-controlling energy is the energy considered primarily responsible for determining the morphology and established empirically. Crystal growth is a process off-equilibrium. In the equilibrium form, the central distances are proportional to the specific surface energy, and for very small crystals the growth form is expected to resemble the equilibrium form closely. The attachment energy is considered to be the habit-controlling energy of the growth form, and the central distances are taken proportional to it. (The central distances are the lengths of the straight line segments drawn from the center of the crystal perpendicular to the faces.) Thus the lower the attachment energy, or equivalently the higher the slice energy (that is the amount of energy contained in that growth layer), the strongest the bonding pattern, the lower the growth rate, and the more important the face (7–9, 14–18). The optimal molecular composition of a primary surface is the one with the lowest attachment energy (9–12,14–18).

Leaving entropy effects out of consideration, the PBC method does not rely on any approximations. Energy quantities can be computed, free from ad hoc or adjustable parameters and free from approximations, using exact, analytic, closed-form expressions (21). In this work, the nearest-neighbor approximation suffices for the purpose of comparison, i.e., for deciding whether the energy quantity of a given surface is smaller or larger than the corresponding energy quantity of another surface. Hence the broken-bond energies are reliable as global indicators of the relative, i.e., not the absolute, strengths of the various slice and attachment energies.

The morphological modification caused by external factors can be assessed from the knowledge of the growth conditions. The integrated effect of the kinetics can in general be expressed in the process of quantifying the surface-environment interaction, and it will modify the growth rates, i.e., the central distances. Apart from this, the PBC theory can take, and has taken, explicitly into account surfaces that reconstruct (5,9,22) and hydrate (9,23,24).

Whether or not a primary surface will actually appear on the growth form, and to which extent it will dominate the morphology, depend directly on the central distances and the angles between them. The central distances in turn are the growth rates as they are calculated from the attachment energies of the structure, and as they are modified by the environmental factors.

PBCs in hexagonal ice

The unit cell of hexagonal ice ($P6_3/mmc$, $a = 4.519$ and $c = 7.357$ Å) contains four water molecules, considered to be represented by their respective oxygen atoms listed in Table 1. Oxygen-oxygen bonds are in tetrahedral coordination. Each oxygen atom has four bonds in the first coordination sphere with bond lengths denoted as p and q and listed in Table 2. (Subsequently each oxygen atom has six bonds of bond length 4.519 Å in the second coordination sphere, etc. Bonds in coordination spheres higher than the first are ignored because they are not considered as strong bonds.) Fig. 6 shows the four oxygen atoms and for each atom the four bonds.

The hydrogen atoms play no role in the PBC analysis for several reasons: first, the determination of the space group relies on the oxygen positions, as the hydrogen positions do not follow the above space group; second, the growth units of ice are entire water molecules, and since they cannot be cleaved at the surface, individual hydrogen atoms play no role in the molecular composition of a growth layer; third, any given hydrogen atom is never linked to more than two oxygen atoms, it can be topologically replaced by a link, providing no additional structural information; fourth, the study is

TABLE 1 Fractional axial coordinates *x, y, z* of the positions of the four oxygen atoms in the unit cell

	x	*y*	*z*
O1	0.3333	0.6667	0.0622
O2	0.6667	0.3333	0.5622
O3	0.6667	0.3333	−0.0622
O4	0.3333	0.6667	0.4378

TABLE 2 Strong bonds between water molecules (oxygen atoms) in the first coordination sphere

O1—O4	*p*	O3—O2[0 0 −1]	*p*
O1—O3	*q*	O3—O1	*q*
O1—O3[0 1 0]	*q*	O3—O1[1 0 0]	*q*
O1—O3[−1 0 0]	*q*	O3—O1[0 −1 0]	*q*
O2—O3[0 0 1]	*p*	O4—O1	*p*
O2—O4	*q*	O4—O2	*q*
O2—O4[1 0 0]	*q*	O4—O2[0 1 0]	*q*
O2—O4[0 −1 0]	*q*	O4—O2[−1 0 0]	*q*

Cell indices are in square brackets. When no cell indices are mentioned, the 0-cell is assumed. Bond lengths $p = 2.763$ Å, $q = 2.765$ Å.

concerned with the topological nature of the AFP-ice interaction based on the bonding pattern in terms of the two-dimensional PBC matching, wherein the charge distribution plays no explicit role; and fifth, as mentioned earlier, the nearest-neighbor approximation suffices for obtaining ratios of growth rates, so that the surface charge distributions entering the absolute values of the surface energies are beyond scope.

The difference between the *p* and *q* bond strengths is negligible since the respective bond lengths differ by 0.002 Å. The primary distinction between the *p* and *q* bonds lies in symmetry properties: whereas the *q* bonds of each oxygen atom are symmetrically related, the *p* bond is symmetrically distinct.

The PBCs and strongly bonded surfaces of hexagonal ice are derived graph-theoretically by the program FFACE (9–11) and listed in Table 3. Each chain begins with an oxygen in the 0-cell and ends with an identical oxygen in cell [*uvw*], indicating the PBC direction. More PBCs exist in the ice structure in symmetrically equivalent directions. The listed PBCs suffice to construct exhaustively the molecular compositions of all strongly bonded surfaces. In the case of ice, the PBCs have a very simple form.

Strongly bonded ice surfaces

Table 4 lists in summary all the directions in which chains were found, together with the strongly bonded surfaces, as obtained from intersecting PBCs. When the combined molecular compositions of the strongly bonded surfaces satisfy the flatness condition, the generated growth layers are admissible as primary surfaces (7–12,14–18,21,23,25,26).

As can be easily seen, there exist PBCs in Table 3 in intersecting directions that define geometrically the (111) face in Table 4. In none of the possible combinations can lattice translations oblique to (111) be avoided. The molecular compositions in the {111} family of eight strongly bonded surfaces belong to category iv as illustrated in Fig. 4. They violate the flatness condition and are unable to maintain the well-defined unique (111) surface orientation (together with the symmetrically equivalent orientations). In the unlikely case such surfaces occur on the ice habit, they would be molecularly roughened.

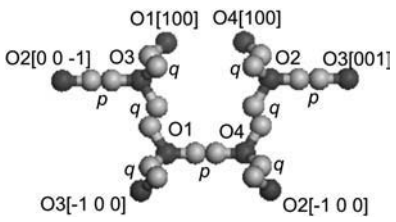

FIGURE 6 Unit cell of hexagonal ice projected on a plane perpendicular to the *b* axis and the strong bonds (*p*,*q*,*q*,*q*) in the first coordination sphere of each oxygen in the unit cell. Each strong bond consists of two O-O links, and each such link is mediated by two hydrogen atoms. Dark balls: oxygen atoms; light balls: hydrogen atoms.

TABLE 3 The PBCs of hexagonal ice in symmetrically unique directions

O1—*q*—O3—*q*—O1[100]
O2—*q*—O4[100]—*q*—O2[100]
O1—*q*—O3[010]—*q*—O1[010]
O2—*q*—O4—*q*—O2[010]
O1—*p*—O4—*q*—O2—*p*—O3[001]—*q*—O1[001]
O1—*p*—O4—*q*—O2[−1 0 0]—*p*—O3[−1 0 1]—*q*—O1[001]
O1—*p*—O4—*q*—O2[010]—*p*—O3[011]—*q*—O1[001]
O1—*p*—O4—*q*—O2[010]—*p*—O3[011]—*q*—O1[011]
O1—*q*—O3[010]—*p*—O2[0 1 −1]—*q*—O4[0 1 −1]—*p*—O1[0 1 −1]
O1—*q*—O3—*p*—O2[0 0 −1]—*q*—O4[1 0 −1]—*p*—O1[1 0 −1]
O1—*q*—O3[010]—*p*—O2[0 1 −1]—*q*—O4[1 1 −1]—*p*—O1[1 1 −1]

The *p* and *q* strong bonds of Table 2 are indicated. Multiple chains in the same direction are in sequence.

The AFP action on the secondary ice surfaces amounts to surface reconstruction through one-dimensional PBC matching, as studied by Strom et al. (5). We now concentrate on the molecular compositions of the primary surfaces: the basal face (001), the primary prism (100), and the primary pyramid (101). Due to the simplicity of the ice structure, only a single molecular composition corresponds to each strongly bonded surface, and hence only a single growth layer is possible for each primary surface orientation: d_{002}, d_{100}, and d_{101}, shown edge-on in Fig. 7 on a plane perpendicular to [010].

In what follows, the molecular composition of face (*hkl*) is denoted by a unit cell that generates that surface when it is repeated in directions parallel to (*hkl*). The (*hkl*) unit cell can be defined in various ways, their molecular content differing only by lattice translations parallel to the face. The PBC bonds need not be indicated for the purpose of defining the surface composition unambiguously. For that reason it suffices to express the (*hkl*) unit cell as a set of molecules between curly brackets, according to the conventional notation used in set theory.

Basal face

The reflection conditions of the space group limit the (001) growth layer to a thickness $d_{002} = 0.5 \times d_{001}$. Therefore only PBCs with one-half the molecular content of the unit cell are admissible. The molecular contents of the PBCs found in directions [100] and [010] (see Table 3) are depicted in Fig. 7. The (001) surface composition obtained from the PBCs (see Table 4) is

TABLE 4 Chain directions [*uvw*] and face indices (*hkl*) of strongly bonded surfaces constructed from the chain directions (Hartman (17,18))

Form	(*hkl*)	[*uvw*]//(*hkl*)			
Primary surfaces					
Prism {100}	(100)	[010]	[001]	[011]	[0 1 −1]
	(010)	[100]	[001]	[101]	[1 0 −1]
	(1 −1 0)	[001]	[110]	[111]	[1 1 −1]
Pyramid {101}	(101)	[010]	[1 0 −1]	[1 1 −1]	
	(1 0 −1)	[010]	[101]	[111]	
	(011)	[100]	[0 1 −1]	[1 1 −1]	
	(0 1 −1)	[100]	[011]	[111]	
	(1 −1 1)	[1 0 −1]	[011]	[110]	
	(1 −1 −1)	[101]	[110]	[0 1 −1]	
Basal face {001}	(001)	[100]	[010]		
Roughened surface					
Pyramid	(111)	[1 0 −1]	[0 1 −1]		

Faces with symmetrically identical orientations are grouped together. Primary forms satisfy ''flatness''. Roughened surface violates the flatness condition.

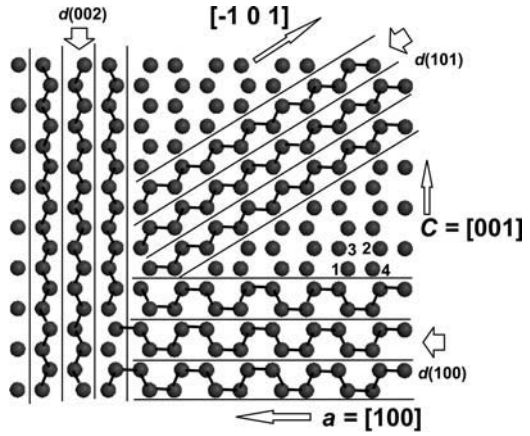

FIGURE 7 Three stacked growth layers of each of the primary surface configurations basal face d_{002}, prism d_{100}, and pyramid d_{101} are shown edge-on in a projection perpendicular to the [010] direction. Straight thin lines indicate the slice boundaries of the molecular compositions. The growth layers $d_{002} = d_{001}/2$ alternate between two different but symmetrically equivalent molecular compositions, each of which contains two oxygen atoms, that is, half the unit cell content (as determined by the extinction conditions of the space group). The oxygen atoms 1–4 in the unit cell are marked and the lattice periods [100], [001], and [−1 0 1] parallel, respectively, to d_{002}, d_{100}, and d_{101} are indicated by arrows.

depicted in Fig. 8. The growth layer d_{002} can be generated by two symmetrically related composition blocks, {O1, O3} or {O2, O4}. The former is shown face-on in Fig. 8 on the (001) face. The basal face grows by these alternating growth layers, each of which includes one-half of the unit cell content (7–12).

Primary prism

Form {100} denotes the collection of symmetrically identical surfaces (100), (010), (1,1 0), and their opposites (−1 0 0), (0 −1 0), (−1 1 0). The molecular contents of the PBCs found in directions [010], [001], [011], and [0 1 −1] (see Table 3) are depicted in Fig. 7. The (100) surface composition obtained from the PBCs (see Table 4) is depicted in Fig. 9. There are many ways of combining these chains to form (alternative) molecular compositions for the growth layer d_{100}. All possible combinations are crystallographically permissible in satisfying the flatness criterion and lead to one distinct molecular composition block for the primary prism surface: {O1,

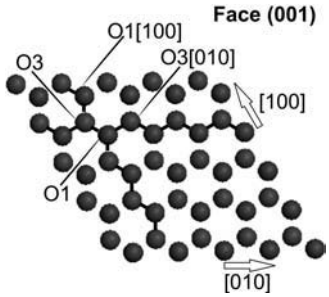

FIGURE 8 Primary surface configuration (001), i.e., the basal face, shown face-on in terms of the constituent PBCs in [100] and [010]. Balls are oxygen atoms; links are strong bonds. The indicated PBCs are repeated by lattice translations, indicated by arrows, to form a network. The orientation of the surface configuration network is predetermined as [100] × [010] = (001). The lattice periods [100] and [010] are marked by arrows.

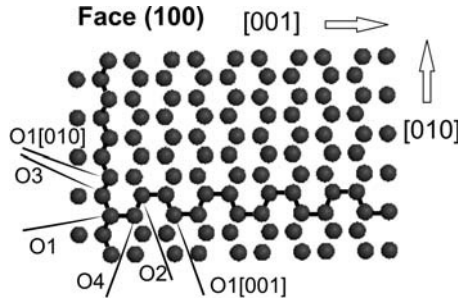

FIGURE 9 Primary surface configuration (100), i.e., the primary prism, shown face-on in terms of the constituent PBCs in [001], [010], [011], and [0 1 −1]. Any two of these PBCs suffice to define the growth layer. Balls are oxygen atoms; links are strong bonds. The indicated PBCs are repeated by lattice translations, indicated by arrows, to form a network. The orientation of the surface configuration network is predetermined as (100). The lattice periods [001], [010], [011], and [0 1 −1] are marked by arrows. Only the PBC O1-O3-O1[0 −1 0] is shown in the [010] direction; the PBC O2-O4-O2[010] is omitted for clarity of presentation.

O2, O3, O4}. The (infinite) growth layer d_{100} is generated by translating this block along at least two of the directions [010], [001], [011], [0 1 −1]. Any pair of intersecting PBCs suffices to define d_{100}. The PBCs in all four directions above are shown in Fig. 9 for completeness. The face indices (100) are theoretically predetermined by the outer product of any pair of the above PBC directions.

Primary pyramid

The bipyramidal form {101} denotes the collection of symmetrically identical surfaces (101), (1 0 −1), (011), (0 1 −1), (1,1,1), and (1,1 −1). The molecular contents of the PBCs found in directions [010], [1 0 −1], and [1 1 −1] (see Table 3) are depicted in Fig. 7. The (101) surface composition obtained from the PBCs (see Table 4) is depicted in Fig. 10. There are many ways of combining these chains to form (alternative) molecular compositions for the growth layer d_{101}.

Combinations of the PBC O2-O4-O2[010] with either of the PBCs in [1 0 −1] or [1 1 −1] violate the flatness criterion. Combinations of the PBC O1-O3-O1[0 -1 0] with either of the PBCs in [1 0 −1] or [1 1 −1], as well as a combination of the last two PBCs, lead to one valid and distinct molecular

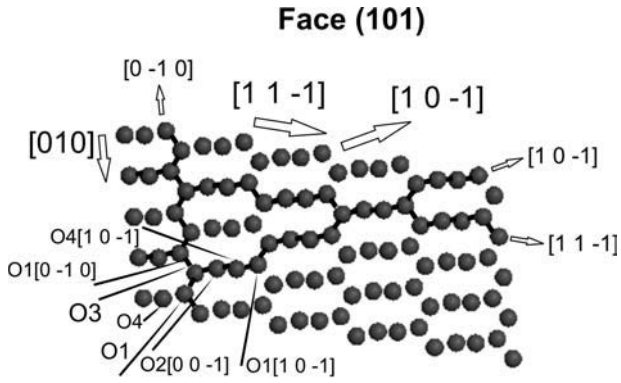

FIGURE 10 Primary surface configuration (101), i.e., the primary pyramid, shown face-on in terms of the constituent PBCs in [010], [1 0 −1], and [1 1 −1]. Balls are oxygen atoms; links are strong bonds. The indicated PBCs are repeated by lattice translations, indicated by arrows, to form a network. The orientation of the surface network is predetermined as (101). The lattice periods of [010], [1 0 −1], and [1 1 −1] are marked by arrows.

composition block for the primary prism surface: {O1, O2[0 0 −1], O3, O4}. The latter three PBCs are indicated in Fig. 10 because they feature in the molecular composition of the (101) surface. The PBC O2-O4-O2[010] is absent from Fig. 10 because it does not participate in any PBC combinations satisfying the flatness condition. The (infinite) growth layer d_{101} is generated by translating this block along at least two of the lattice directions [010], [1 0 −1], [1 1 −1]. Any pair of intersecting PBCs suffices to define d_{101}. The PBCs in all three directions above are shown in Fig. 10. The face indices (101) are theoretically predetermined by the outer product of any pair of the above PBC directions.

Structural morphology from attachment energies of primary surfaces

Slice and attachment energies in terms of bond strengths are tabulated in Table 5 for the primary surfaces of Table 4 and Figs. 7–10 (7–9, 14–18,25,26). The crystal energy is the sum of the slice and attachment energies, and it is a constant equal to $2p + 6q$, independently of the orientation (*hkl*). The energy quantities in the last two columns are normalized to $p = q = 1$.

A comparison between Figs. 9 and 10 shows that the (100) prism with four PBCs in its molecular composition is more strongly bonded than the (101) pyramid, which has only three PBCs in its molecular composition. This is easily seen from the difference in the growth layer energies of Table 5; the slice energy difference between the prism and the basal face, $2(p - q)$, is negligible since $p \sim q$; however, the difference between the prism and the pyramid, q, is substantial. The difference in attachment energy between the strongest-bonded configuration d_{100} and the next strongest d_{002} is $E_{att}(100) - E_{att}(002) = 2(q - p)$, which is negligible because $p \sim q$, whereas the difference between d_{100} and d_{101}, i.e., $E_{att}(100) - E_{att}(101) = -q$, is more pronounced. Therefore the primary pyramid has a weaker bonding structure than either the basal face or the prism that is of comparable bond strength. Thus the pyramid is expected to have a substantially higher growth rate and consequently a lower morphological importance.

The structural morphology of hexagonal ice is constructed according to the rule-of-thumb prescription of taking the growth rates of the various theoretical flat faces proportional to their respective attachment energies (7,8,14–18,25,26) and taking into account geometrical factors. It is shown schematically (not to scale) in Fig. 11. We find that the (101) primary pyramid (normalized growth rate 3 in Table 5) does not appear on the growth form because it happens to lie just below the threshold of appearance by a small amount. The (101) face does not appear due to geometry and due to the relatively high attachment energy of (101). Therefore (101) is suppressed by the more strongly bonded basal face (001) and primary prism (100) in the structural morphology of ice. Should some external factor cause a reduction in the growth rate of (101) bringing it below the theoretical threshold, then we may observe the primary pyramid (101) on the growth form of ice.

AFP-induced surface pinning via two-dimensional PBC matching predicted theoretically

External factors, like the AFP-substrate interaction, can enhance or suppress some growth rates preferentially; since the resulting reduction in the growth rates affects some faces more than others, the morphology undergoes a modification. The stronger the interaction of a crystal surface with the molecular species in the ambient phase, the more pronounced the resulting surface enhancement. The natural morphology of ice when it grows out of water is an example of the surface interaction with the water molecules. The exact growth form of natural ice depends on the level of supercooling, and it likely deviates from the structural morphology shown in Fig. 11.

TABLE 5 Slice and attachment energies of the primary surfaces expressed in terms of bonds, and in terms of bonds normalized to bond strength = 1, in order of decreasing slice energy; $E_{slice} + E_{att} = E_{crystal} = 2p + 6q$ = constant, units per unit cell per mol

Face	E_{slice} (p,q)	E_{att} (p,q)	E_{slice} (norm)	E_{att} (norm)
Basal face (001)	$6q$	$2p$	6	2
Prism (100)	$2p + 4q$	$2q$	6	2
Pyramid (101)	$2p + 3q$	$3q$	5	3

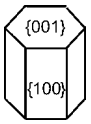

FIGURE 11 Approximate structural morphology, i.e., the morphology for which the structure is responsible in the absence of any external influence based on calculated structural attachment energies (the primary pyramid is absent for geometrical and energetic reasons).

The most effective mechanism of enhancing preferentially some primary surfaces, of which the face indices are predetermined, is to occupy crystallographic sites and block parts of a surface. The approaching crystallizing units are delayed or prevented from reaching crystallographic sites and becoming incorporated in the crystal structure. For the crystallization process to continue, the crystallizing units need to overcome the AFP's blocking action. This delaying effect affects some surface molecular compositions preferentially, causing the relative growth rates of the engaged surfaces to decrease. As a consequence, the surface area in that orientation increases. The AFP-induced surface pinning via two-dimensional PBC matching enhances some faces at the cost of suppressing others and hence modifies the morphology.

Thus the strong binding of AFP molecules to the surface of ice according to the aforementioned effect can cause step pinning, which will hinder the movement of steps by covering the kinks at the surface. This is illustrated schematically in Fig. 12, showing a statistical distribution of insect-type IBSs on a primary surface. The two-dimensional insect-type IBS possesses the necessary periodicity properties to match simultaneously the existing lattice translations in two intersecting directions.

In comparing theory with experiment, the predicted characteristics of the AFP-induced mechanism modifying the ice morphology are recaptured as follows:

i. Engagement by the IBS exclusively on the primary ice surfaces. The two-dimensional insect-type of IBS is characterized by a two-dimensional, planar structure with regularly arranged binding intervals matching the lattice periods of ice. The lattice periods matched by the IBS-binding intervals should correspond to the theoretical strong-bonding directions of the observed ice facets featuring in the morphology. Since the IBS is equipped to modify the morphological

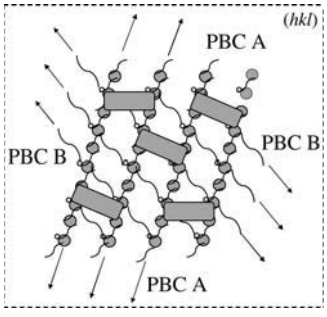

FIGURE 12 Schematic illustration of a statistical distribution of insect-type IBSs on a primary surface in category i, resulting in the pinning effect through two-dimensional PBC matching.

importance of the primary ice surfaces, the affected surfaces must have the theoretically predetermined face indices: (001), (100), and (101).

ii. Constancy of the orientations of the engaged surfaces under all experimental conditions. Because the face indices of the primary surfaces are fixed by the intersecting PBC directions, the IBS of the AFP is unable to adjust the surface orientations. In other words, the insect AFP action should be limited to the morphological important predetermined surface orientations, without affecting the face indices themselves.

iii. Alignment of the IBS along strong-bonding directions on the ice surface. The particular structure of the IBS is expected to be aligned along the intersecting PBCs on the engaged surface.

iv. Possible correlation between IBS properties and face indices of the engaged primary surfaces. Structure matching between the IBS and the lattice periods of the primary surfaces means that the (attractive) interaction between the ice substrate and the AFP should be locally optimized. The interaction-enhancing mechanisms depend of the AFP's capacity to grip and block lattice cites on the ice surface. Hydrogen bonding, ice lattice occupation, and van der Waals interactions have been suggested as possible mechanisms.

The basal face and the primary prism have the highest density of PBCs per unit surface area, whereas the primary pyramid has the smallest fraction per unit area accessible to water molecules. IBS structures prone to lattice occupation are expected to reinforce the basal face and the primary prism. On the other hand, when hydrogen bonding becomes the dominant mechanism of interaction between the IBS and the ice surface, the primary pyramid (101) could likely appear on the growth form.

The reason for this can be seen in the difference in attachment energies between basal face or prism as compared to the primary pyramid. Because each p or q bond is mediated by a hydrogen atom, the attachment energies are a direct measure of the number of dangling hydrogen bonds on the surface. We see that (100) and (001) have the same number of hydrogen atoms available for bonding with the AFP, that is, 2 hydrogen atoms per surface area of the unit cell, whereas (101) has one more, that is, 3 hydrogen atoms per surface area of the unit cell.

The increased amount of hydrogen bonding available on the primary pyramid (101) should enable an IBS prone to hydrogen bonding to bind to the (101) surface in preference to (001) or (100).

v. Possible activation of the primary pyramid (101) by the insect IBS. In accordance with the above theoretical predictions, the ice morphology triggered by the insect-type AFP need not be limited to a combination of the basal face (001) and the primary prism (100), as is customarily assumed in the literature. The insect AFP may well trigger, albeit not exclusively, the primary pyramid (101).

vi. Absence of the (111) bipyramid should be observed as a consequence of the theoretical prediction that (111) should be susceptible to surface roughening.

Docking simulation

Three insect AFP proteins (TmAFP, spruce budworm isoform 501 (Sbw501), and spruce budworm isoform 337 (Sbw337)) (20,27,28) are first manually docked without relaxation to the ice planes with approximate alignment with corresponding ice atoms. The object of the docking is the closest spatial fit using a rigid ice surface and a rigid AFP surface. They were actual crystal structures as indicated in the articles by Liou et al. (20), Leinala et al. (27), and Leinala et al. (28). Their Protein Data Bank codes are TmAFP-1EZG; Sbw50 -1M8N; Sbw337-1L0S.

The second step involves the optimization of the manual alignment using an automated least-squares overlap optimization algorithm. Finally, root mean-square deviation (rmsd) values are computed and listed in Table 6. The following bare ice substrates were used as input: all three primary surface configurations, analyzed in this work, consisting of the basal plane (001), the primary prism (100), and the primary pyramid (101). Moreover, some secondary surface configurations with low crystallographic indices were used: the secondary pyramids (102) and (201) and two variants of the secondary prisms (110) and (120), see Strom et al. (5).

TABLE 6 Root mean-square deviations of the docking simulation (in Å)

Ice face	sbw501	sbw337	TmAFP
001	0.680	0.751	0.605
100	0.550	0.580	0.554
101	1.232	1.102	0.931
102	1.601	1.664	1.568
110A	1.281	1.253	1.139
110B	1.185	1.234	1.204
120A	1.620	1.787	1.591
120B	2.649	2.854	2.505
201	2.128	2.383	2.108

All three insect AFPs (TmAFP, Sbw501, and Sbw337) possess a similar β-helix structure with Thr-X-Thr motif on its IBS. For TmAFP, there are 10 Thr residues. For Sbw501, there are 11 Thr residues. For Sbw337, there are 9 Thr residues. Although there are some discrepancies in the results which are most likely due to experimental structures of the AFPs, the general trend is clear: (100) and (001) planes are the best matching all three proteins. For higher index planes, the match gradually becomes worse.

The docking reported above was done on the basis of an integrated set of criteria including lattice occupancy and hydrogen bonding. From the docking and a host of other experiments, we know that the TmAFP binds by a two-dimensional binding mechanism along two directions. According to the rmsd values from the docking results, the TmAFP shows a comparable affinity to the other two insect AFPs for the basal face and the prism and a closer affinity for the (101) pyramid. Because hydrogen bonding and lattice occupancy were combined in the docking criteria used, the docking results may not be sensitive to the special relation between a hydrogen bonding IBS and the appearance of the (101) primary pyramid mentioned in points iv and v in the previous section.

RESULTS AND DISCUSSION

It has long been recognized in the literature (13) that the insect AFP's capacity to suppress freezing is due to its capacity to grip firmly on the ice lattice by using its two-dimensional periodic binding intervals adjusted to the ice lattice constants. Taking the primary prism (100) as an example, the spruce budworm AFP producing the hexagonal disk type (29) morphology in Fig. 13 has regular binding intervals in two directions equal to ~4.5 and 7.5 Å, matching the periods of the strong bonding directions [010] and [001].

The characteristic morphology of ice grown from most insect AFP solutions is hexagonal plates (13,29). In com-

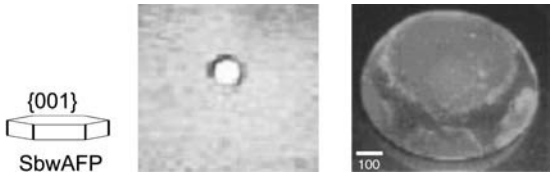

FIGURE 13 Morphology observed in the presence of the spruce budworm AFP (SbwAFP). Left, schematic; right, Figs. 1 and 3 of Graether et al. (29).

parison with the structural or the natural morphology, these ice crystallites exhibit a strongly pronounced basal face (001) and a morphologically much weakened primary prism (100), cf. Fig. 11. In all ice crystallites grown as basal and primary prismatic forms, resulting from layer-by-layer growth, triggered, e.g., by the Spruce budworm AFP, no deviation from the $\{001\}$ and $\{100\}$ indices has been observed under all experimental conditions.

One presumed exception to the hexagonal disk form is found in the action of the TmAFP, the presence of which gives rise to a pyramidal ice habit. It is traditionally held that the action of the insect TmAFP is deviant in causing a pyramidal rather than a disk-shaped morphological modification, whereas all other known insect AFPs cause a hexagonal plate habit. The question arises as to whether the mechanism of morphological modification in the case of the TmAFP is exceptional; that means, whether the IBS of the TmAFP acts on secondary ice surfaces by an exceptional mechanism or on primary ice surfaces by surface pinning through two-dimensional PBC matching, just like the remaining insect-type IBSs. What this question amounts to is whether the pyramidal ice form observed in the presence of the TmAFP is one of the secondary pyramids with variable indices ($h0l$) or the primary pyramid (101).

Fig. 14 shows the ice bipyramid (30) triggered by the TmAFP, which has consistently a stubby lemon shape, showing no variation in the apical angle, so that the TmAFP gives rise to a pyramid of fixed indices. The lemon-shaped ice bipyramid produced by the TmAFP is not elongated like the predominant (201) or higher-indexed pyramids observed in connection with the fish AFPs. From the assortment of pyramidal shapes in Fig. 14, it can be seen that this bipyramid matches well the primary surface (101). Also here we see that in all ice crystallites grown as primary pyramidal

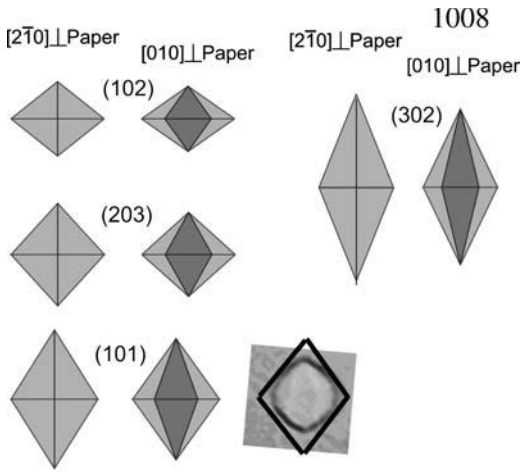

FIGURE 14 Outlines of various pyramidal forms compared with the ice bipyramid produced by the TmAFP (Fig. 7 *E* of Walthen et al. (30)) that matches the (101) primary ice pyramid undergoing a morphological modification through two-dimensional PBC matching leading to surface pinning.

forms triggered by the TmAFP, resulting from layer-by-layer growth, no deviation from the $\{101\}$ indices has been observed under all experimental conditions. Thus the TmAFP action is by no means exceptional.

According to Liou et al. (20), the TmAFP has a high tendency to form hydrogen bonds with an ice surface. This result agrees with our theoretical observation that there are 30% more unbonded hydrogen atoms on the (101) than in the other primary surfaces, pointing to an increased interaction between the IBS of the TmAFP and the (101) primary pyramid.

CONCLUSIONS

A PBC-theoretic analysis of the insect AFP-ice system led for the first time to a comprehensive explanation of the morphological modification of the ice crystallites brought about by the insect AFPs. The insect-type IBS engages the primary surfaces of ice and causes a morphological modification by the two-dimensional PBC-matching mechanism leading to surface pinning. A good deal of experimental evidence supports the theoretical predictions. The primary surfaces have fixed face indices because they contain intersecting strong-bonding directions. The insect AFPs consistently trigger ice crystallites with the primary surfaces and no other than the primary surfaces. No variations of or deviations from the primary face indices have been observed, despite vast differences in experimental conditions.

For the insect-type IBS to trigger the aforementioned surface pinning effect, it would need to distribute itself statistically over the engaged surface and match the lattice translations of the PBCs defining the surface molecular composition. The predicted alignment of this two-dimensional IBS, which is capable of matching the ice lattice in two directions, along the PBCs of the engaged surface is repeatedly observed experimentally.

In previous studies the appearance of pyramidal forms was associated with the presence of the fish AFPs or AFPGs that have a lower level of activity. The appearance of ice bipyramids in the presence of the TmAFP has puzzled researchers, because this protein is an insect AFP and has behaved in all other respects like the other insect AFPs, exhibiting a high level of activity. The PBC-theoretic analysis leads to the conclusion that the TmAFP bipyramids are not the same as the bipyramids obtained by the fish-type IBS. Whereas the latter produces bipyramids with variable secondary surface orientations, the former produces bipyramids with fixed surface orientations, equal in all cases to the primary (101) surface.

The molecular composition of the primary pyramid (101) growth layer, as determined by the intersecting PBCs, has a higher density by 30% of hydrogen-dangling bonds than the molecular compositions of the basal face (001) and the primary prism (100). This excess of hydrogen bonds on the (101) surface implies that an insect-type IBS prone to hy-

drogen bonding is more likely to engage the (101) pyramid, whereas an insect-type IBS prone to lattice occupation is more likely to engage a combination of the basal face (001) and the primary prism (100). Indeed, according to experimental reports, the TmAFP has a larger IBS, more capable of forming hydrogen bonds. Therefore the appearance of (101) bipyramids can be explained by the IBS properties of the TmAFP.

An additional (heuristic) explanation for the engagement of the (101) primary surfaces by the TmAFP could be that (101) has less accessible surface area than (001) and (100) to water molecules, so that the AFP can more easily block the (101) surface. This explanation is in line with the docking results of Sbw337, Sbw501, and TmAFP on various ice substrates; there the TmAFP shows a closer affinity than other insect AFPs for the (101) pyramid.

The (111) bipyramid has never been observed on the ice crystallites under all experimental conditions, in agreement with the theoretical prediction according to which (111) belongs to category iv, and hence should undergo surface roughening as illustrated in Fig. 4.

Finally, the mechanism of surface pinning through two-dimensional PBC matching is consistent with the superior activity exhibited by the insect AFPs, in contrast to the surface reconstruction caused by the fish AFPs and AFPGs.

We are indebted to Dr. Zhang Keqin and Dr. Li Dawei for assistance in preparing the figures.

REFERENCES

1. Wilson, P. W., and J. P. Leader. 1995. Stabilization of supercooled fluids by thermal hysteresis proteins. *Biophys. J.* 68:2098–2107.
2. Du, N., and X. Y. Liu. 2002. Controlled ice nucleation in microsized water droplet. *Appl. Phys. Lett.* 81:445–447.
3. Du, N., X. Y. Liu, and C. L. Hew. 2003. Ice nucleation inhibition. Mechanism of antifreeze by antifreeze protein. *J. Biol. Chem.* 278: 36000–36004.
4. Liu, X. Y., and N. Du. 2004. Zero-sized effect of nanoparticles and inverse homogeneous-like nucleation principles of freezing and antifreeze. *J. Biol. Chem.* 279:6124–6131.
5. Strom, C. S., X.-Y. Liu, and Z. Jia. 2005. Ice surface reconstruction as AFP-induced morphological modification mechanism. *J. Am. Chem. Soc.* 127:428–440.
6. Mutaftschiev, B. 1993. Handbook of Crystal Growth, Vol. 1. D. T. J. Hurle, editor. North-Holland, Amsterdam. 189–247.
7. Hartman, P. 1969. The Dependence of Crystal Morphology on Crystal Structure: Growth of Crystals, Vol. 7. N. N. Sheftal, editor. Consultants Bureau, New York. 3–18.
8. Hartman, P. 1973. Crystal Growth. An Introduction: Crystal Growth. P. Hartman, editor. North-Holland, Amsterdam. 367–401.
9. Strom, C. S., R. F. P. Grimbergen, P. Bennema, H. Meekes, M. A. Verheijen, L. V. P. Vogels, and M. Wang. 1999. Ionic crystals in the Hartman-Perdock theory with case studies: ADP ($NH_4H_2PO_4$)-type structures and gel-grown fractal ammonium chloride (NH_4Cl). *In* Molecular Modeling Applications in Crystallization. A. S. Myerson, editor. Cambridge University Press, New York. 228–312 (and references therein).
10. Strom, C. S. 1980. Graph-theoretic construction of periodic bond chains. I. General case. *Zeit. f. Kristallographie*. 153:99–113.
11. Strom, C. S. 1981. Graph-theoretic construction of periodic bond chains. II. Ionic case. *Zeit. f. Kristallographie*. 154:31–43.
12. Strom, C. S. 1985. Finding F-faces by direct chain generation. *Zeit. f. Kristallographie*. 172:11–24.
13. Jia, Z., and P. L. Davies. 2002. Antifreeze proteins: an unusual receptor-ligand interaction. *Trends Biochem. Sci.* 27:101–106 (and references therein).
14. Hartman, P., and W. Perdok. 1955. On the relations between structure and morphology of crystals. I. *Acta Crystallogr.* 8:49–52.
15. Hartman, P., and W. Perdok. 1955. On the relations between structure and morphology of crystals. II. *Acta Crystallogr.* 8:521–524.
16. Hartman, P., and W. Perdok. 1955. On the relations between structure and morphology of crystals. III. *Acta Crystallogr.* 8:525–529.
17. Hartman, P. 1958. The Madelung constants of slices and chains, with an application to the CdI_2 structure. *Acta Crystallogr.* 11:365–369.
18. Hartman, P. 1958. The equilibrium forms of crystals. *Acta Crystallogr.* 11:459–464.
19. Greather, S. P., and B. D. Sykes. 2004. Cold survival in freeze-intolerant insects. The structure and function of beta-helical antifreeze proteins. *Eur. J. Biochem.* 271:3285–3296.
20. Liou, Y. C., A. Tocilj, P. L. Davies, and Z. Jia. 2000. Mimicry of ice structure by surface hydroxyls and water of a beta-helix antifreeze protein. *Nature.* 406:322–324.
21. Strom, C. S., and P. Hartman. 1989. Comparison between Gaussian and exponential charge distributions in Ewald surface potentials and fields: NaCl, aragonite, phlogopite. *Acta Crystallogr. A.* 45:371–380.
22. Strom, C. S., X. Y. Liu, and M. Wang. 2000. Solution-induced reconstructive epitaxial nucleation on pseudo-flat surfaces of fractal gel-grown ammonium chloride. *J. Phys. Chem. B.* 104:9639–9644.
23. Strom, C. S. 1999. Ewald ionic surface maps gauging the effect of solvent interaction on crystal morphology by surface x-ray diffraction of potassium dihydrogen phosphate (KDP). *J. Phys. Chem. B.* 103: 1133–1145.
24. Strom, C. S. 2001. Validity of Hartman-Perdok PBC theory in prediction of crystal morphology from solution and surface x-ray diffraction of potassium dihydrogen phosphate (KDP). *J. Cryst. Growth.* 222:298–310.
25. Hartman, P. 1956. An approximate calculation of attachment energies for ionic crystals. *Acta Crystallogr.* 9:569–572.
26. Hartman, P. 1956. The morphology of zircon and potassium dihydrogen phosphate in relation to the crystal structure. *Acta Crystallogr.* 9:721–727.
27. Leinala, E. K., P. L. Davies, and Z. Jia. 2002. Crystal structure of β-helical spruce budworm antifreeze protein shows intimate surface complementarity to ice. *Structure.* 10:619–627.
28. Leinala, E. K., P. L. Davies, D. Doucet, M. G. Tyshenko, V. Walker, and Z. Jia. 2002. A β-helical antifreeze protein isoform with increased activity: structural and functional insights. *J. Biol. Chem.* 277:33349–33352.
29. Graether, S. P., M. J. Kuiper, S. M. Gagné, V. K. Walker, Z. Jia, B. D. Sykes, and P. L. Davies. 2000. Beta-helix structure and ice-binding properties of a hyperactive antifreeze protein from an insect. *Nature.* 406:325–328.
30. Walthen, B., M. Kuiper, V. Walker, and Z. Jia. 2003. New model for simulating 3D crystal growth and its application to the study of antifreeze proteins. *J. Am. Chem. Soc.* 125:729–737.